Investigating the Sensitivity of Tetra-hybrid Microfluidic Flow Under Magnetic Field Localization

Shabbir Ahmad [1, 2,3*], Elizaldo Domingues dos Santos [1, 4,5], Kashif Ali [2], Moin-ud-Din Junjua [6,7*], Farhan Lafta Rashid [8], Ahmed S Hendy [9,10], Noureddine Elboughdiri [11], Saad Alshahrani [12,13]

[1.] Graduate Program of Ocean Engineering, School of Engineering, Universidade Federal do Rio Grande, Rio Grande, Brazil, Italia Avenue, km 8, 96201-900.
[2] Department of Basic Sciences and Humanities, Muhammad Nawaz Sharif University of Engineering and Technology, Multan 60000, Pakistan
[3] Institute of Geophysics and Geomatics, China University of Geosciences, Wuhan 430074, China
[4]. Programa de Pós-Graduação em Modelagem Computacional/LMCE, Escola de Engenharia, Universidade Federal do Rio Grande - FURG, 96203900, Rio Grande - RS, Brasil
[5]. FURG, Escola de Engenharia, Rio Grande - RS, Brasil
[6] School of Mathematical Sciences, Zhejiang Normal University, Jinhua 321004, China
[7]. Department of Mathematics, Ghazi University, Dera Ghazi Khan 32200, Pakistan
[8]. Petroleum Engineering Department, College of Engineering, University of Kerbala, Karbala 56001, Iraq
[9] Department of Computational Mathematics and Computer Science, Institute of Natural Sciences and Mathematics, Ural Federal University, 19 Mira St., Yekaterinburg 620002, Russia
[10]. Department of Mechanics and Mathematics, Western Caspian University, Baku, 1001, Azerbaijan
[11]. Chemical Engineering Department, College of Engineering, University of Ha'il, P.O. Box 2440, Ha'il 81441, Saudi Arabia.
[12]. Department of Mechanical Engineering, College of Engineering, King Khalid University, P.O. Box 394, Abha 61421, Saudi Arabia
[13]. Center for Engineering and Technology Innovations, King Khalid University, Abha 61421, Saudi Arabia

[*] Correspondence Authors Email: shabbiraleem@cug.edu.cn, moinuddin@zjnu.edu.cn

Abstract: This study explores the sensitivity of tetra-hybrid microfluidic flow to localized magnetic fields, focusing on their impact on flow dynamics, stress distribution, and thermal behavior. A rectangular cavity (aspect ratio 4:1) filled with a tetra-hybrid nanofluid is analyzed, with the top and bottom walls moving in the same direction. A confined magnetic field, structured in horizontal and vertical strips, is introduced to assess its influence. An alternating-direction implicit method has been used to enhance numerical stability and efficiently solve the discretized governing equations, and the single-phase model has been used to model the fluid. Furthermore, custom MATLAB codes, employing the Stream-Vorticity formulation and a finite difference method, are used to solve the governing equations. The findings demonstrate that increasing the magnetic field strength up to 500 enhances heat transfer by 65%. Among nanostructures, a 20% silver concentration yields the highest improvement, increasing the Nusselt number by 313%, followed by SWCNT (54%), TiO_2 (43%), and Cu (31%). Regarding skin friction, silver and TiO_2 reduce it by 65%, while Cu lowers it by 52%. However, SWCNT exhibits an opposite effect, increasing skin friction by 138% due to its elongated structure, which enhances flow resistance.

Keywords: Magnetic field; Reynolds Number; Nanoparticles; Vortex dynamics; Tetra-hybrid microfluidic flow

1. Introduction

Vortices play a crucial role in fluid mixing and mass transport, making them essential in flow studies. They form due to velocity differences and appear in hurricanes, tornadoes, and airflow over wings. Understanding vortices helps explain various natural phenomena across different environments. Common examples include smoke rings, dust devils, and cyclones. Studying vortices is crucial due to their natural presence and technical applications. The investigation of vortex dynamics in lid-driven cavities holds significant practical value across various industries, particularly in improving mixing efficiency and optimizing thermal regulation. In chemical engineering, managing vortex formation enhances the performance of mixing reactors by ensuring a more uniform distribution of reactants. Similarly, in thermal management, insights into vortex behavior contribute to the development of advanced cooling systems for electronic devices, facilitating more effective heat dissipation. Ahmad et al. [1] applied the alternating direction implicit (ADI) method to study the influence of localized magnetic fields on the flow dynamics and thermal behavior of nanofluids. Using a stream–vorticity formulation, they solved the dimensionless form of the governing partial differential equations. Their findings revealed that higher Reynolds numbers enhance both the magnetic field effects and heat transfer rates, while the Lorentz force induces parallel vortices along the vertical walls. In a related study, Ali et al. [2] examined the impact of localized magnetic fields on the flux distribution of hybrid nanofluids within a magnetically driven enclosure. They employed a single-phase model (SPM) to classify hybrid nanofluids and numerically solved the governing PDEs to evaluate the system's behavior. The findings show that a counter-rotating vortex created by the localized magnetic field in the flow splits apart the other vortex and becomes stronger as a result. The vortex tends to fill a large portion of the cavity and elongates along the direction of the localized magnetic field. In the heat gradient close to the enclosure's horizontal walls, the magnetic field weakens. The regularity of the isotherm pattern is distorted by the more vigorous mixing of the fluid layer at varying temperatures brought on by the faster-moving lids.

The application of a magnetic field particularly in electrically conducting fluids—can significantly influence the fluid motion through the Lorentz force. This interaction can suppress turbulence, alter vortex structures, and control heat and mass transfer within the cavity. Such effects are not only important in fundamental fluid dynamics research but also have direct industrial relevance. Wang et al. [3] developed a permanent magnet–based flow velocity meter that uses electrode current rather than voltage for measurement. A theoretical model was derived linking output current with velocity, conductivity, magnet properties, and electrode placement, supported by finite element simulations. Experiments confirmed that the new design reduces output drift by 92% compared to voltage sensors, achieving an R2=0.998R^2 = 0.998 over 0–0.875 m/s. The effect of bidirectional magnetic field modulation on STPM machines with fractional-slot concentrated windings was analyzed by Liu et al. [4] Using an equivalent PM–MMF permeance model, torque components were quantified, considering stator/rotor slotting and validated via Maxwell stress tensor analysis to explain torque production. Luo et al. [5] developed a simplified parametric model to predict the nonlinear hysteresis behavior of magnetorheological fluids containing micron-sized carbonyl iron particles. Large-amplitude shear tests at varying currents were used for parameter identification through genetic optimization. Compared with Bouc–Wen and hyperbolic tangent models, the new approach required fewer parameters while improving predictive accuracy for automotive damping and suspension systems. By incorporating temperature into feature sequences, Zheng et al. [6] enhanced hybrid prediction models for magnetic encoders. Feature engineering minimized error interference, yielding superior compensation accuracy in

experiments and demonstrating a practical method for improving encoder reliability. Two asymmetric flux-reversal permanent magnet linear machines (AFR-PMLMs) for long-stroke applications were proposed by Li et al. [7]. Asymmetric excitation allowed effective utilization of second-order harmonic MMF, significantly increasing thrust force density. Analytical modeling based on an improved MMF–permeance approach was validated with finite element analysis. Zhu et al. [8] introduced dual-excitation permanent magnet linear machines (DEPMLMs) for extended travel applications. By generating second-order harmonics in both primary excitation MMF and secondary excitation permeance, thrust force density was markedly enhanced. Analytical models and finite element results showed performance improvements exceeding 98.1% and 79.1% over AFR-PMLM and switched-flux PMLM designs, respectively. Further studies can be found in the following literature [9-11].

Hybrid nanofluids offer greater stability, combined material effects, and improved heat transfer performance compared to conventional nanofluids. These unique features make them highly useful across diverse fields, including materials science, transportation, medical technologies, and energy systems. Ahmad et al. [12] numerically investigated the flow and thermal behavior of hybrid nanofluids using a finite volume approach in MATLAB, considering parameters like magnetic field strength, Reynolds number, and nanoparticle concentration. Results reveal that magnetized fields induce vortex structures, significantly affecting skin friction and heat transfer. Silver nanoparticles show the highest enhancement, while alumina and titanium dioxide exhibit weaker effects. Additionally, localized magnetic fields have a stronger influence on flow behavior than uniform fields. Grace et al. [13] investigated heat transfer in a stenosed artery, where the governing fluid transport equations were transformed into ordinary differential equations using similarity variables. The resulting system was solved in MATLAB with the BVP4C solver. According to the study, magnetic fields stabilize flow patterns and facilitate heat transfer by aligning nanoparticles, while higher curvature improves convective heat transfer despite initial flow resistance. Furthermore, thermal radiation increases heat transmission through improving energy absorption and decreasing the thickness of the boundary layer. The flow dynamics and heat transfer properties of a Cu-CNT-Graphene-TiO_2/WEG-Blood hybrid nanofluid were examined by Kumar et al. [14] in the presence of linear thermal radiation and an angled magnetic field. This research has important implications for military, biomedical, and engineering applications. The ODE45 integration technique was used to solve the governing nonlinear differential equations for momentum, energy, and concentration using the ANFIS-PSO model. This resulted in important information about the hybrid nanofluid's flow and thermal behavior. Ahmad et al. [15] used machine learning to investigate vortex dynamics in a 2:1 horizontal cavity under localized magnetic fields. The ADI method and the Stream-Vorticity formulation resolve governing equations. According to the results, the Nusselt number (Nu) is greatly increased by stronger magnetic fields; Ag and Cu show the most increases (53%), while TiO_2 shows the least impact (37%).

In an enclosure with movable lids, Ali et al. [16] examined the effects of the Lorentz force and nanoparticle concentration on heat transmission and discovered that both factors improve heat transfer and raise shear stress on the lower wall. The term "localized magnetic fields" refers to magnetic fields that are contained inside specific regions or places. Localized magnetic fields differ from uniform magnetic fields in that they are concentrated and focused within certain places. The scientific community is very interested in this topic because of its importance and applicability Kumar et al. [17] studied the flow of boundary layers over porous wedges in nanofluids, ternary hybrid nanofluids, and hybrid nanofluids, under heat radiation and a transverse magnetic field. AA7072, magnesium oxide, zirconium oxide, and various combinations of polyethylene glycol-water are used as base fluids in

the cases. The 4th-order Runge-Kutta method with the Shooting technique is used to solve the governing ODEs. Results show that ternary hybrid nanofluids achieve higher Nusselt number transfer rates, while hybrid nanofluids exhibit greater skin friction. Elboughdiri et al. [18] investigated the stagnation point Darcy-Forchheimer flow of a trihybrid nanofluid (THNF) comprising oxytactic and gyrotactic microorganisms around a spinning sphere in the presence of a magnetic field, viscous dissipation, and Joule heating. n order to compare performance, it takes into account heat generation, higher-order chemical interactions, and the Hamilton–Crosser model. The results have implications for environmental applications, biomedical engineering, and sophisticated cooling systems. Elboughdiri et al. [19] investigated the two-dimensional, continuous flow of a ferrofluid through a porous substance whose thermal conductivity varies with temperature. Using Nield's boundary conditions, they examined how magnetic dipoles, Brownian motion, radiation, and thermophoresis affected a stretching sheet. The results reveal that raising the ferrofluid parameter boosts temperature but decreases velocity, whilst increasing viscosity further reduces velocity. Elboughdiri et al. [20] analyzed the thermal and flow characteristics of radiating copper–ethylene glycol nanofluids in an unsteady 2D stagnation point flow over a horizontal electromagnetic actuator, and developed a new EMHD-based dissipative second-grade nanofluid model. The findings demonstrate that flow and heat transfer are significantly impacted by nanoparticle size and loading. Elboughdiri et al. [21] examined the impact of magnetic devices on the peristaltic transport of a viscoelastic nanofluid in curved concentric tubes, resembling endoscopic flow in living organs. A non-Newtonian Casson liquid polymer governs the fluid dynamics, with silver and alumina nanoparticles dispersed in a clay-based fluid.

Tri-hybrid nanofluids are distinguished by their composition, which consists of the dispersion of three different types of nanoparticles inside a base fluid. Metals, carbon-based compounds, and metal oxides are all possible materials for nanoparticles to be made of. The integration of multiple nanoparticle types provides a chance to increase thermal and physical properties beyond those seen in typical nanofluids. Trihybrid nanofluids have been extensively studied for their potential applications in a wide range of sectors, including electronic cooling, heat transfer, biomedical engineering, and energy storage systems. Ongoing research focusses on the potential applications of nanofluids. The major goal is to improve their performance and develop innovative applications across multiple disciplines. Kumar et al. [22] studied a tri-hybrid AA7072 + SWCNT + MWCNT nanofluid model with H2O as the base fluid under magnetohydrodynamic flow at 100°C and 500°C. Elboughdiri et al. [23] investigated, under long-wavelength and low Reynolds-number assumptions, how chemical reactions affect heat transfer and peristaltic pumping of nanofluids in a convergent channel. Mathematica 11.0 is used to derive numerical solutions for temperature, velocity, nanoparticle concentration, and stream function, which are then examined for a range of rheological parameters. The findings indicate that while raising the heat source parameter increases temperature and concentration of nanoparticles, it slows flow. Raju et al. [24] explored the flow and heat transfer properties of a nanofluid in a porous channel that expands or contracts with different permeabilities when exposed to heat radiation. In cylindrical, spherical, and platelet configurations, two ternary hybrid nanofluids—one containing graphene, carbon nanotubes, and aluminum oxide, and the other including copper, silver, and copper oxide—are examined. The bvp5c solver in MATLAB is used to solve the highly nonlinear system after it has been modified using similarity transformations. In their analysis of the heat and velocity transfer rate, Dinesh Kumar et al. [25] looked at a number of factors, including buoyancy and suction, on a stretching sheet through a porous media. The resulting Ordinary differential equations were solved using the ODE45 numerical technique and the boundary value problem solver. Elboughdiri et al. [26] explored innovative microchannel heat sinks (MCHSs)

with arc-curved microchannels carved on segmented circular heat sinks, which had six separate spiral microchannel segments. The impact of these partitions on the pressure drops (ΔP) and Nusselt number (Nu) is examined. The results demonstrate much greater Nu values than traditional MCHSs, followed by increased ΔP.

The novelty of this study lies in investigating tetra-hybrid nanofluid flow under localized magnetic fields with a combined horizontal and vertical strip configuration, which has not been explored previously. The work highlights the synergistic effects of multiple nanoparticles on heat transfer and skin friction, identifying the most effective combinations for thermal enhancement and flow control. Additionally, the integration of the alternating-direction implicit method with custom Stream-Vorticity MATLAB codes provides a robust and efficient numerical framework for analyzing complex microfluidic behavior.

2. Problem Description

Fig. 1 depicts a 2D horizontal cavity with a 4:1 aspect ratio, featuring magnetic strips integrated into the form of strips. These strips generate a magnetic field that significantly influences the system's behavior. To analyze this, researchers use the single-phase model (SPM), a thermodynamic-based tool, combined with the stream-vorticity formulation. This approach solves the momentum, energy, and mass conservation equations in a 2D Cartesian coordinate system.

2.1. Basic Assumptions

The study is based on several key assumptions. The magnetic field intensity H is confined within specified horizontal and vertical strips. The cavity has vertically insulated walls, while the horizontal walls are maintained at different temperatures, with both lids moving along the positive x-axis. The working fluid is a tetra-hybrid nanofluid composed of Ag, SWCNT, TiO_2, and Cu nanoparticles.

3. Mathematical Formulation

The dimensional representation of the following equations is given below: [27]:

Continuity equation:

$$\frac{\partial \bar{U}}{\partial x}+\frac{\partial \bar{V}}{\partial y}=0, \tag{1}$$

Momentum equation:

$$\frac{\partial \bar{U}}{\partial t'}+\left(\bar{V}\frac{\partial \bar{U}}{\partial y}+\bar{U}\frac{\partial \bar{U}}{\partial x}\right)=-\frac{1}{\rho_{tet-hnf}}\frac{\partial P}{\partial x}+\left(\upsilon_{tet-hnf}+\frac{\kappa}{\rho}\right)\left(\frac{\partial^2 \bar{U}}{\partial y^2}+\frac{\partial^2 \bar{U}}{\partial x^2}\right)+\frac{\bar{\mu}_o \bar{M}}{\rho_{tet-hnf}}\frac{\partial \bar{H}}{\partial x}+\frac{\kappa}{\rho}\frac{\partial \phi}{\rho y}, \tag{2}$$

$$\frac{\partial \bar{V}}{\partial t'}+\left(\bar{U}\frac{\partial \bar{V}}{\partial x}+\bar{V}\frac{\partial \bar{V}}{\partial y}\right)=-\frac{1}{\rho_{tet-hnf}}\frac{\partial P}{\partial y}+\left(\upsilon_{tet-hnf}+\frac{\kappa}{\rho}\right)\left(\frac{\partial^2 \bar{V}}{\partial x^2}+\frac{\partial^2 \bar{V}}{\partial y^2}\right)+\frac{\bar{\mu}_o \bar{M}}{\rho_{tet-hnf}}\frac{\partial \bar{H}}{\partial y}+\frac{\kappa}{\rho}\frac{\partial \phi}{\rho x}, \tag{3}$$

Angular Momentum:

$$\frac{\partial \phi}{\partial t'}+\left(\bar{U}\frac{\partial \phi}{\partial x}+\bar{V}\frac{\partial \phi}{\partial y}\right)=-\frac{2\kappa}{\rho j}\phi+\frac{\gamma}{\rho j}\left(\frac{\partial^2 \phi}{\partial x^2}+\frac{\partial^2 \phi}{\partial y^2}\right)+\frac{\kappa}{\rho}\left(\frac{\partial \bar{V}}{\partial x}-\frac{\partial \bar{U}}{\partial y}\right)-\frac{\kappa}{\rho}\frac{\partial \phi}{\partial x} \tag{4}$$

Energy Equation:

$$\frac{\partial T}{\partial t'}+\frac{\left(\rho c_p\right)_{tet-hnf}}{k_{tet-hnf}}\left(\bar{U}\frac{\partial T}{\partial x}+\bar{V}\frac{\partial T}{\partial y}\right)+\left(\frac{\bar{\mu}_o}{k_{tet-hnf}}\right)T\frac{\partial \bar{M}}{\partial T}\left(\bar{V}\frac{\partial \bar{H}}{\partial y}+\bar{U}\frac{\partial \bar{H}}{\partial x}\right)$$
$$=\nabla^2 T+\left(\frac{\bar{\mu}_{tet-hnf}}{k_{tet-hnf}}\right)\left\{2\left(\frac{\partial \bar{U}}{\partial x}\right)^2+\left(\frac{\partial \bar{V}}{\partial x}+\frac{\partial \bar{U}}{\partial y}\right)^2+2\left(\frac{\partial \bar{V}}{\partial y}\right)^2\right\}. \tag{5}$$

Upon eliminating the pressure component, the following is obtained:

$$\frac{\partial}{\partial t'}\left(\frac{\partial \bar{U}}{\partial y}-\frac{\partial \bar{V}}{\partial x}\right)+\bar{V}\frac{\partial}{\partial y}\left(\frac{\partial \bar{U}}{\partial y}-\frac{\partial \bar{V}}{\partial x}\right)+\bar{U}\frac{\partial}{\partial x}\left(\frac{\partial \bar{U}}{\partial y}-\frac{\partial \bar{V}}{\partial x}\right)$$
$$=\upsilon_{tet-hnf}\left(\frac{\partial^2}{\partial x^2}+\frac{\partial^2}{\partial y^2}\right)\left(\frac{\partial \bar{U}}{\partial y}-\frac{\partial \bar{V}}{\partial x}\right)+\frac{\kappa}{\rho}\left(\frac{\partial^2}{\partial x^2}+\frac{\partial^2}{\partial y^2}\right)+\left(\frac{\partial\left(\frac{\bar{\mu}_0\bar{M}}{\rho_{tet-hnf}}\frac{\partial \bar{H}}{\partial x}\right)}{\partial y}-\frac{\partial\left(\frac{\bar{\mu}_0\bar{M}}{\rho_{tet-hnf}}\frac{\partial \bar{H}}{\partial y}\right)}{\partial x}\right). \tag{6}$$

3.1 Boundary Conditions

The analysis is constrained by the following dimensional boundary conditions.

Right and left vertical walls (adiabatic):

$$\left.\begin{array}{l}\bar{U}(0,y)=\bar{U}(4L,y)=0,\quad \left(\frac{\partial T}{\partial x}\right)_{x=0}=\left(\frac{\partial T}{\partial x}\right)_{x=4L}=0,\\ \bar{V}(0,y)=\bar{V}(4L,y)=0;\ \phi(0,y)=\phi(4L,y)=0;\end{array}\right\}\quad 0<y<L \tag{7a}$$

Upper Horizontal Wall:

$$\left.\begin{array}{l}\bar{U}(x,L)=V_0,\quad T(x,L)=T_C,\\ \bar{V}(x,L)=0;\ \phi(x,L)=n_0\left(\frac{\partial \bar{U}}{\partial y}\right)_{y=L}\end{array}\right\}\quad 0<x<4L \tag{7b}$$

Lower Horizontal Wall:

$$\left.\begin{array}{l}\bar{U}(x,0)=V_0,\quad T(x,0)=T_h,\\ \bar{V}(x,0)=0;\ \phi(x,0)=n_0\left(\frac{\partial \bar{U}}{\partial y}\right)_{y=0}\end{array}\right\}\quad 0<x<4L. \tag{7c}$$

3.2 Thermophysical Analysis of Tetra-Hybrid vs. Conventional Nanofluids

In this section, we elucidate the thermophysical qualities of the tetra-hybrid nanofluids, which are an integral part of our analysis of heat transport phenomena. Specifically, we focus on a unique set of thermophysical properties relevant to tetra-hybrid nanofluids comprising Ag-SWCNT-TiO_2-Cu nanoparticles. These properties, including specific heat, density, viscosity, and thermal conductivity, are validated based on existing literature [28-32]. **Table 1** presents a comparison of the thermophysical properties of tetra-hybrid nanofluids and conventional nanofluids.

The analysis is carried out using the following dimensionless variables:

$$\xi = \frac{x}{L},\ y = \frac{y}{L},\ u = \frac{\psi}{V_0},\ v = \frac{\psi}{V_0},\ \theta = \frac{T - T_c}{\Delta T},\ H = \frac{H}{H_0},\ t = \frac{V_0}{L}t' \tag{8}$$

Equations 3 and **Equation 4** lead us to conclude that:

$$\frac{\partial J}{\partial t} + u\frac{\partial J}{\partial \xi} + v\frac{\partial J}{\partial \eta} = \left(\rho_{tet\_hnf} \big/ \rho_f\right)\left(\mu_f \big/ \mu_{tet\_hn}\right)\frac{1}{\mathrm{Re}}(1+C)\nabla^2 J + \frac{Mn}{\left(\rho_{tet\_hn} \big/ \rho_f\right)} H\left(\frac{\partial H}{\partial \eta}\cdot\frac{\partial \theta}{\partial \xi} - \frac{\partial H}{\partial \xi}\cdot\frac{\partial \theta}{\partial \eta}\right) + \frac{C}{\mathrm{Re}}\nabla^2 N, \tag{9}$$

$$\nabla^2\theta = \mathrm{Pr}*\left(\rho_{tet\_hnf} \big/ \rho_f\right)\left(\frac{\mu_f}{\mu_{tet\_hnf}}\right)*\left(\frac{(\rho c_p)_{tet\_hnf}}{(\rho c_p)_f}\right)\mathrm{Re}*\left(\frac{1}{\left(\frac{\mu_f}{\mu_{tet\_hnf}}\right)\left(\rho_{tet\_hnf} \big/ \rho_f\right)}\right)\left\{\frac{\partial \theta}{\partial \xi}\frac{\partial \psi}{\partial \eta} - \frac{\partial \theta}{\partial \eta}\frac{\partial \psi}{\partial \xi}\right\} + \mathrm{Pr}*\left(\frac{\mu_f}{\mu_{tet\_hnf}}\right)\left(\rho_{tet\_hnf} \big/ \rho_f\right)*\left(\frac{(\rho c_p)_{tet\_hnf}}{(\rho c_p)_f}\right)*\frac{Mn}{\left(\rho_{tet\_hnf} \big/ \rho_f\right)}\mathrm{Re}$$

$$*\left(\frac{1}{\left(\frac{\mu_f}{\mu_{tet\_hnf}}\right)\left(\rho_{tet\_hnf} \big/ \rho_f\right)}\right)EcH(\varepsilon - \psi)\left\{\frac{\partial H}{\partial \xi}\frac{\partial \psi}{\partial \eta} - \frac{\partial H}{\partial \eta}\frac{\partial \psi}{\partial \xi}\right\} + \mathrm{Pr}*\left(\rho_{tet\_hnf} \big/ \rho_f\right)\left(\frac{\mu_f}{\mu_{tet\_hnf}}\right)*\left(\frac{(\rho c_p)_{tet\_hnf}}{(\rho c_p)_f}\right)Ec\left\{\left(\frac{\partial^2 \psi}{\partial \eta^2} - \frac{\partial^2 \psi}{\partial \xi^2}\right)^2 + 4\left(\frac{\partial^2 \psi}{\partial \xi \partial \eta}\right)^2\right\}, \tag{10}$$

$$\frac{\partial N}{\partial t} + \left(u\frac{\partial N}{\partial \zeta} + v\frac{\partial N}{\partial \eta}\right) = -\frac{2C}{\mathrm{Re}}\phi + \left(1+\frac{C}{2}\right)\frac{1}{\mathrm{Re}}\left(\frac{\partial^2 N}{\partial \zeta^2} + \frac{\partial^2 N}{\partial \eta^2}\right) + \frac{C}{\mathrm{Re}}\left(\frac{\partial v}{\partial \zeta} - \frac{\partial u}{\partial \eta}\right), \tag{11}$$

where,

$$H_1(\xi,\eta) = H_0\left\{\tanh A_1(\xi - \xi_1) - \tanh A_2(\xi - \xi_2)\right\},\ H_2(\xi,\eta) = H_0\left\{\tanh A_1(\eta - \eta_1) - \tanh A_2(\eta - \eta_2)\right\}$$

in the strips defined by $\xi_1 \le \xi \le \xi_2;\ 0 \le \eta \le 1$, and $\eta_1 \le \eta \le \eta_2;\ 0 \le \xi \le 1$, respectively.

$$\text{Finally, } H(\xi,\eta) = H_1(\xi,\eta) + H_2(\xi,\eta) \tag{12}$$

We utilize the stream-vorticity formulation, which modifies **Equations 1-3** as follows:

$$u = \frac{\partial \psi}{\partial \eta},\ v = \frac{\partial \psi}{\partial \xi} \text{ and } \left(\frac{\partial u}{\partial \eta} - \frac{\partial v}{\partial \xi}\right) = -\omega \text{ or } \left\{\left(\frac{\partial^2 \psi}{\partial \xi^2} + \frac{\partial^2 \psi}{\partial \eta^2}\right) = -\omega\right\}. \tag{13}$$

Similarly, the non-dimensional boundary conditions are as follows:

Left and Right Vertical Walls (Thermally Insulated):

$$\left.\begin{array}{l} u(0,\eta)=u(4,\eta)=0, \quad \left(\frac{\partial \theta}{\partial \xi}\right)_{\xi=0}=0, \left(\frac{\partial \theta}{\partial \xi}\right)_{\xi=4}=0, \\ v(0,\eta)=v(4,\eta)=0, \quad N(0,\eta)=N(4,\eta)=0 \end{array}\right\} \qquad 0 < \eta < 1 \tag{14a}$$

Upper Horizontal Wall:

$$\left.\begin{array}{l} u(\xi,1)=1, \quad \theta(\xi,1)=0, \\ v(\xi,1)=0; \; N=n\left(\dfrac{\partial u}{\partial \eta}\right)_{\eta=1} \end{array}\right\} \qquad 0<\xi<4 \qquad (14b)$$

Lower Horizontal Wall:

$$\left.\begin{array}{l} u(\xi,0)=1, \quad \theta(\xi,0)=1, \\ v(\xi,0)=0; \; N=n\left(\dfrac{\partial u}{\partial \eta}\right)_{\eta=0} \end{array}\right\} \qquad 0<\xi<4. \qquad (14c)$$

3.3 Relevant Physical Quantities

In this study, the primary variables examined are skin friction (CfRe) and the Nusselt number (Nu), defined as follows:

$$\mathrm{Nu}=\frac{qL}{k_{tet\_hnf}\Delta T} \quad \text{and} \quad \mathrm{CfRe}=\frac{2\tau}{\rho_{tet\_hnf}v_0^2}$$

where,

$\tau=\mu_{tet\_hnf}\left(\dfrac{\partial U}{\partial \eta}\right)\Big|_{\eta=0,L}$ shear stress $\qquad$ $q=-k_{tet\_hnf}\left(\dfrac{\partial T}{\partial \eta}\right)\Big|_{\eta=0,L}$ heat flux

The dimensionless parameters yield the following results:

$$\mathrm{CfRe}=\left(\frac{\rho_f}{\rho_{tet\_hnf}}\right)\left(\frac{\mu_{tet\_hnf}}{\mu_f}\right)\frac{\partial u}{\partial y}, \text{ and } N_u=\left(\frac{k_{tet\_hnf}}{k_f}\right)\frac{\partial \theta}{\partial y}.$$

4. Numerical Methodology

The transformed **Equations 9-13**, along with the boundary conditions (**Equation 14**), are numerically solved using the pseudo-transient approach. In this method, time serves as an iteration parameter until convergence is reached. For further details, refer to [15]. Further, **Fig. 2** depicts the numerical model used for the alternating direction implicit (ADI) scheme.

4.2 Comparing the Numerical Scheme with Benchmarks

Fig. 3 presents a comparative analysis of horizontal velocity profiles at various horizontal locations (x = 0.25, 0.5, and 0.75) within a given fluid domain. The plot juxtaposes "Our Results" with benchmark data from "Asia et al. [33]" at each x-location. Solid lines represent "Our Results," while dashed lines with asterisks correspond to the "Asia et al. [33]" data. Consistent color coding (red for x = 0.25, black for x = 0.5, and blue for x = 0.75) facilitates easy visual comparison between the two datasets at each respective x-location. This direct comparison allows for the assessment of the agreement between "Our Results" and the established data from Asia et al., crucial for validating the numerical simulation of fluid flow behavior. The excellent agreement observed between the two datasets confirms the accuracy and reliability of our numerical procedure.

Table 2 presents a comprehensive overview of the key thermophysical properties of the constituent materials used in the formulation of Ag-SWCNT-TiO2-Cu-water-based nanofluids. These properties are critical for evaluating and optimizing their performance in specific applications. The table highlights essential parameters, including particle size, which influences dispersion stability and heat transfer behavior; thermal conductivity, a determinant of heat transport efficiency; specific heat capacity, which affects the nanofluid's energy storage capability; viscosity, which plays a vital role in fluid flow and pumping power requirements; and density, which impacts buoyancy and flow dynamics. A uniform grid has been carefully selected for the numerical simulations, ensuring an evenly spaced distribution of points across the computational domain.

The grid step size $h = 0.01$ has been chosen based on the findings from a comprehensive grid independence study, as illustrated in **Fig. 4.** This study was conducted to determine the optimal balance between computational accuracy and efficiency by evaluating how changes in grid resolution impact the stability and convergence of the solution. The selected step size provides sufficient accuracy while minimizing computational cost, ensuring that the numerical results are not significantly influenced by further refinement of the grid.

5. Results and Discussion

This section presents a visual and analytical representation of streamlines, isotherms, and microrotation patterns within a cavity, utilizing both tables and figures. These visualizations provide insight into temperature distribution and fluid flow characteristics. To further contextualize the numerical results, contours of stress factors and gradients for streamlines, isotherms, and microrotations are also generated. The stress factor, directly related to the shear stress at any given point in the flow, is visualized across the entire flow domain using contour plots. Tabulated data includes the skin friction coefficient (CfRe) and Nusselt number (Nu) calculated at the top and bottom horizontal walls. These data are specific to a configuration where both the lower and upper horizontal lids of the enclosure translate in the positive x-direction. Within the enclosure, a unique magnetic field configuration is employed, consisting of discrete strips, designated as $\xi_1 \le \xi \le \xi_2;\ 0 \le \eta \le 1$, and, $\eta_1 \le \eta \le \eta_2;\ 0 \le \xi \le 4$. This study investigates the influence of several key parameters on the flow and heat transfer characteristics. These parameters include: Reynolds Number $(1 \le \mathrm{Re} \le 10)$, Magnetic Number $(0 \le \mathrm{Mn} \le 500)$, and Microrotation Parameter $(0 \le \mathrm{C} \le 5)$.

5.1 Effects of Magnetizing Force

Fig. 5 illustrates the impact of magnetic field strength, shown by strips in region $1.5 - L \le \xi \le 2.5 + L;\ \ 0 \le \eta \le 1$, and $0.4 - L \le \eta \le 0.6 + L;\ \ 0 \le \xi \le 4$ on parameters like isotherms, streamlines, microrotation, temperature gradients, stress factors, and microrotation gradients. Vortex rotation is linked to the movement of a horizontal cavity's lids, driven by a mechanical setup. Without a magnetic field, the flow remains simple and follows a predictable pattern, resulting in uniform stress contours due to the absence of external forces disrupting the motion. As the magnetic number (Mn) increases, the applied magnetic force interacts with the fluid, altering its movement and introducing complexities in the flow. This leads to irregular stress contours as different regions experience varying magnetic influences. Stronger magnetic fields intensify these effects, creating more intricate flow structures and increasing stress in areas where the fluid deforms around the magnetic

field lines. This behavior highlights the significant role of magnetic fields in manipulating flow dynamics and stress distribution in microfluidic systems. **Fig. 6** shows that at Mn=0, isotherms are closer to the cavity's upper lid, with even spacing and smooth temperature gradients, indicating consistent fluid temperature. As Mn increases from 50 to 500, isotherms become irregular, and temperature gradients turn non-uniform, suggesting reduced temperature uniformity within the fluid. The physical reasoning behind this behavior lies in the interaction between the magnetic field and the fluid's motion. At Mn = 0, there is no magnetic influence, so heat transfer occurs primarily through conduction and natural convection, leading to smooth and evenly spaced isotherms near the upper lid. As Mn increases, the Lorentz force alters the fluid flow by introducing additional resistance and modifying the velocity field. This disrupts the natural convection patterns, causing localized variations in heat transfer rates. Consequently, isotherms become irregular, and temperature gradients become non-uniform, indicating areas of enhanced and suppressed thermal transport within the cavity. **Fig. 7** shows that magnetic fields strongly influence microrotation, with higher magnetic numbers (Mn) increasing its strength and spread. This is due to the magnetic force disrupting flow dynamics. The study highlights that magnetic fields alter microrotation gradient distribution. Accurate flow prediction requires considering magnetic effects on microrotation and other flow parameters. The overall suppression of microrotation is due to the stabilizing effect of the magnetic field, which dampens rotational motion. However, localized enhancements occur in regions where magnetic field gradients induce secondary flow structures.

5.2 Impact of the Reynolds Number

Fig. 8 shows streamlines and stress factor contours for flow at varying Reynolds numbers (Re) with Mn = 50, Pr = 6.8, $\phi_1 = \phi_2 = \phi_3 = \phi_4 = 0.02$ and C = 1. As Re increases, streamlines grow more complex and disordered due to stronger inertial forces, potentially causing turbulence. Stress factor contours reveal higher stress near walls, where shear stress is most pronounced. **Fig. 9** demonstrates that the Reynolds number has a significant impact on the temperature distribution within the flow regime. At lower Reynolds numbers, the temperature profile remains relatively smooth, with steep gradients localized in specific regions. As the Reynolds number increases, the distribution becomes more complex and uneven. Understanding this behavior is essential for accurately predicting temperature fields, particularly in engineering applications such as heat exchangers or combustion chambers, where it directly influences heat transfer efficiency and overall performance. **Fig. 10** presents the microrotation and its gradient contours in a fluid-filled enclosure for Mn = 5, Pr = 6.8, and C = 1 at various Reynolds numbers. An increase in Re leads to higher microrotation in both the upper and lower regions, indicating faster rotation of fluid particles, likely due to dominant flow effects outweighing microstructural influences. Moreover, higher Reynolds numbers produce more irregular and distorted contours, reflecting increased flow complexity and affecting the spatial distribution of microrotation and its gradients.

5.3 Role of the Micropolar Parameter

Fig. 11 shows that the micropolar characteristics of fluids significantly affect flow patterns and stress distribution. When microrotation is absent, the streamlines and stress factor contours appear more distinct and well-defined. However, with the introduction of microrotation, the flow becomes smoother and more uniform. This can

also lead to the laminar nature of the flow, causing modifications in both the flow pattern and stress distribution. **Fig. 12** shows that the micropolar parameter influences temperature distribution. As the parameter decreases, isotherms become more distorted, and temperature gradient contours cluster near the upper horizontal wall, indicating rapid temperature changes in that region. This occurs because microrotation increases fluid particle collisions, enhancing heat transfer from warmer to cooler areas. **Fig. 13** illustrates the effects of the micropolar parameter on microrotation and its gradient in a flow. The results indicate that variations in the parameter substantially affect both the microrotation patterns and their gradients. Higher parameter values encourage a laminar flow by aligning particles along the field lines, reducing rotational motion, and promoting a more organized flow structure. These findings are particularly valuable for refining models in fields such as astrophysics, engineering, and energy production, especially in the analysis of dusty fluid flows.

5.4 Effect of Different Parameters on Physical Quantities

Table 3 illustrates the effect of increasing the magnetic field strength from zero to 500. As the magnetic field strengthens, the Nusselt number rises noticeably, indicating enhanced heat transfer. The impact on skin friction, however, is even more significant, demonstrating a substantial increase. This indicates that the magnetic field has a stronger influence on skin friction than on the Nusselt number. Similarly, **Table 4** shows the effect of the Reynolds number on both the Nusselt number and skin friction. It is clear that higher Reynolds numbers lead to a marked increase in both quantities, emphasizing the critical role of Reynolds number in determining heat transfer and surface shear stress. **Table 5** presents the effect of the microrotation parameter (C), which measures the intensity of microrotation in the fluid. An increase in C results in a decrease in both the Nusselt number (Nu) and the skin friction coefficient (CfRe). This decline results in lower heat transfer efficiency and a decrease in shear stress. A higher value of C diminishes the temperature gradient and enhances fluid viscosity. By adjusting C, it is possible to regulate heat transfer rates and fluid flow accordingly. **Tables 6–9** clearly indicate that increasing the concentration of nanostructures leads to an increase in the Nusselt number at varying rates, while skin friction generally follows an inverse trend. Among the tested nanostructures, silver exhibits the highest enhancement in the Nusselt number. A 20% increase in silver concentration in water results in a 313% rise in the Nusselt number, whereas SWCNT, titanium dioxide, and copper lead to enhancements of 54%, 43%, and 31%, respectively. This highlights the significant influence of silver nanostructures on heat transfer performance. The primary reason for this behavior is the superior thermal conductivity of silver compared to other nanoparticles, which facilitates enhanced convective heat transfer by reducing thermal resistance and promoting efficient energy exchange between fluid layers. Conversely, a 20% concentration of silver nanoparticles results in a 65% reduction in skin friction, a similar decrease is observed with titanium dioxide, while copper nanostructures reduce skin friction by 52%. However, an opposite trend is noted for SWCNT, which increases skin friction by 138% at the same concentration. This increase in skin friction with SWCNT can be attributed to its elongated tubular structure, which induces additional flow resistance and turbulence near the boundary layer, thereby elevating shear stress. In contrast, the reduction in skin friction observed for silver, titanium dioxide, and copper is primarily due to their ability to enhance fluid lubrication and reduce velocity gradients at the solid-liquid interface.

5.5 Comparative Analysis for the Thermal Characteristics of Different Nanomaterials

Fig. 14 reveals that penta-hybrid fluids outperform in terms of the average Nusselt number, which gives a clear higher performance compared to nano/hybrid or tetra-hybrid nanofluids.

5.6 Role of the Confined Magnetic Field

The magnetic strips can be defined as: $0.5-L<\xi<1.0+L;\ 0<\eta<1,\ 2.0-L<\xi<3.0+L;\ 0<\eta<1,$ and $4.0-L<\xi<4.5+L;\ 0<\eta<1.$ When L is zero, the left and right-hand strips exhibit a fixed width of 0.5 units, while the central strip has a width of 1.00 units. What's interesting is that the nano-structure affects the Nusselt number differently as the parameter L grows, indicating a broader strip, as shown in **Fig. 15**.

6. Concluding Remarks

This study presents a numerical investigation of the interaction between micropolar tetra-hybrid flow in an enclosed domain and an externally applied magnetic field, generated through a configuration of horizontal and vertical strips. The results demonstrate that magnetic field strength, Reynolds number, microrotation parameter, and nanoparticle concentration significantly influence heat transfer and skin friction. An increase in magnetic field strength improves heat transfer, with an even more pronounced effect on skin friction. Similarly, higher Reynolds numbers result in notable rises in both the Nusselt number and skin friction, highlighting their key role in controlling flow behavior. The microrotation parameter (C) adversely impacts heat transfer and skin friction by increasing fluid viscosity. Moreover, the type and concentration of nanoparticles critically affect thermal performance: silver nanoparticles provide the greatest heat transfer enhancement due to their high thermal conductivity, while SWCNTs increase skin friction owing to their tubular geometry. These findings offer valuable guidance for optimizing fluid flow and thermal management in microfluidic and engineering applications.

Acknowledgment: The authors extend their appreciation to the Deanship of Research and Graduate Studies at King Khalid University for funding this work through Large Research Project under grant number RGP.2/387/46.

Data Availability Statement: Data will be provided by the authors upon request.

Authors contribution statement

Shabbir Ahmad: Conceived of the presented idea, developed the mathematical model, designed the numerical simulations, interpreted the results, wrote the initial draft of the manuscript, and supervised the overall research work.

Elizaldo Domingues dos Santos: Contributed to developing the computational methodology, performed the simulations, analyzed the data, and assisted in revising the manuscript.

Kashif Ali: Conducted the parametric studies, validated the numerical models, contributed to interpreting the findings, and assisted in preparing the figures and tables.

Moin-ud-Din Junjua: Developed parts of the numerical code, carried out additional simulations, reviewed the literature, and contributed to drafting and refining the introduction and discussion sections.

Farhan Lafta Rashid: Provided consultation on heat transfer aspects, contributed to the theoretical formulation, and reviewed and revised the manuscript critically for important intellectual content.

Ahmed S. Hendy: Assisted in designing the computational experiments, contributed to the analysis and interpretation of results, and supported editing the entire manuscript.

Noureddine Elboughdiri: Reviewed the thermophysical property data of nanofluids, contributed to validating the numerical approach, and provided expert input on sustainability and energy conservation aspects.

Saad Alshahrani: Performed additional verification tests, contributed to preparing the graphical materials, assisted in interpreting the results, and contributed to revising the manuscript.

References

[1] Ahmad, S., Ali, K., Tayebi, T., et al., "Unveiling the magic of localized magnetic field on vortex dynamics and heat transfer of tetra-hybrid nanofluid in lid-driven cavity: an insightful investigation", *Journal of Thermal Analysis and Calorimetry*, **149**(2), pp. 653-670 (2024) https://doi.org/10.1007/s10973-023-12733-w

[2] Ali, K., Ahmad, S., Ahmad, S., et al., "Impact of magnetic field localization on the vortex generation in hybrid nanofluid flow", *Journal of Thermal Analysis and Calorimetry*, **148**(13), pp. 6283-6300 (2023). https://doi.org/10.1007/s10973-023-12104-5

[3] Wang, Z., Wang, S., Wang, X., et al., "Permanent magnet-based superficial flow velometer with ultralow output drift", *IEEE Transactions on Instrumentation and Measurement*, **72**, pp. 1-12 (2023). https://doi.org/10.1109/TIM.2023.3304692

[4] Wang, C., Liu, J., Han, J., et al., "Analysis of bidirectional magnetic field modulation on concentrated winding spoke-type PM machines", *IEEE Transactions on Transportation Electrification*, **10**(3), pp. 6076-6086 (2023). https://doi.org/10.1109/TTE.2023.3348235

[5] Zhang, G., Luo, J., Sun, M., et al., "A novel reliable parametric model for predicting the nonlinear hysteresis phenomenon of composite magnetorheological fluid", *Smart Materials and Structures*, **34**(3), pp. 035060 (2025). https://doi.org/10.1088/1361-665X/adbf57

[6] Jiang, W., Zheng, B., Sheng, D., et al., "A compensation approach for magnetic encoder error based on improved deep belief network algorithm", *Sensors and Actuators A: Physical*, **366**, pp. 115003 (2024). https://doi.org/10.1016/j.sna.2023.115003

[7] Shen, Y., Li, Z., Zeng, Z., et al., "Quantitative analysis of asymmetric flux reversal permanent magnet linear machine for long excursion application", *IEEE Transactions on Industrial Electronics*, **71**(10), pp. 12781-12792 (2024). https://doi.org/10.1109/TIE.2023.3344854

[8] Shen, Y., Zhu, X., Yang, H., et al., "Design and Evaluation of Dual Excitation Permanent Magnet Linear Machine With Optimal Utilization of Extended Working Harmonics", *IEEE Transactions on Industrial Electronics*, (2025). https://doi.org/10.1109/TIE.2025.3563678

[9] He, D., Xu, H., Wang, Y., et al., "Research on vertical vibration characteristics of rolling mill based on magnetorheological fluid damper absorber", *Mechanical Systems and Signal Processing*, **224**, pp. 112203 (2025). https://doi.org/10.1016/j.ymssp.2024.112203

[10] Jiang, Z., Shi, H., Tang, X., et al., "Recent advances in droplet microfluidics for single-cell analysis", *TrAC Trends in Analytical Chemistry*, **159**, pp. 116932 (2023). https://doi.org/10.1016/j.trac.2023.116932

[11] Ma, N., Fang, X., Zhang, Y., et al., "Enhancing the sensitivity of spin-exchange relaxation-free magnetometers using phase-modulated pump light with external Gaussian noise", *Optics Express*, **32**(19), pp. 33378-33390 (2024). https://doi.org/10.1364/OE.530764

[12] Ahmad, S., Ali, K., Castellanos, H.G., et al., "Complex dynamics of induced vortex formation and thermal-fluid coupling in tri-hybrid nanofluid under localized magnetic field: a novel study", *Scientific Reports*, **13**(1), pp. 21140 (2023). https://doi.org/10.1038/s41598-023-48386-w

[13] Grace, D.S., Durgaprasad, P., and Palencia, J.L.D., "Response surface optimisation on Non-Uniform shapes ternary hybrid nanofluid flow in stenosis artery with motile gyrotactic microorganisms", *Chemical Physics*, **590**, pp. 112539 (2025). https://doi.org/10.1016/j.chemphys.2024.112539

[14] Kumar, M.D., Jawad, M., Ramanuja, M., et al., "Forecasting heat and mass transfer enhancement in magnetized non-Newtonian nanofluids using Levenberg-Marquardt algorithm: influence of activation

energy and bioconvection", *Mechanics of Time-Dependent Materials*, **29**(1), pp. 14 (2025). https://doi.org/10.1007/s11043-024-09739-8

[15] Ahmad, S., Ali, K., Sultan, H.H., et al., "A Breakthrough in Penta-Hybrid Nanofluid Flow Modeling for Heat Transfer Enhancement in a Spatially Dependent Magnetic Field: Machine Learning Approach", *International Journal of Thermophysics*, **46**(1), pp. 1-34 (2025). https://doi.org/10.1007/s10765-024-03467-4

[16] Ali, K., Prakash, M., Jamshed, W., et al., "Imposed magnetic field impact on vortex generation in the laminar nanofluid flow: A computational approach", *International Communications in Heat and Mass Transfer*, **139**, pp. 106469 (2022). https://doi.org/10.1016/j.icheatmasstransfer.2022.106469

[17] Kumar, M.D., Ahammad, N.A., Raju, C., et al., "Response surface methodology optimization of dynamical solutions of Lie group analysis for nonlinear radiated magnetized unsteady wedge: Machine learning approach (gradient descent)", *Alexandria Engineering Journal*, **74**, pp. 29-50 (2023). https://doi.org/10.1016/j.aej.2023.05.009

[18] Elboughdiri, N., Fatima, N., Abd El-Rahman, M., et al., "Characteristics of unsteady thermo-bioconvection chemical reactive stagnation point flow of trihybrid nanofluid around rotating sphere with oxytactic microorganisms", *Case Studies in Thermal Engineering*, **61**, pp. 104981 (2024). https://doi.org/10.1016/j.csite.2024.104981

[19] Elboughdiri, N., Dharmaiah, G., Prasad, J.L.R., et al., "Analysis of a ferromagnetic nanofluid saturating a porous medium with nield's boundary conditions", *Mathematics*, **11**(22), pp. 4579 (2023). https://doi.org/10.3390/math11224579

[20] Elboughdiri, N., Ghernaout, D., Muhammad, T., et al., "Towards a novel EMHD dissipative stagnation point flow model for radiating copper-based ethylene glycol nanofluids: An unsteady two-dimensional homogeneous second-grade flow case study", *Case Studies in Thermal Engineering*, **45**, pp. 102914 (2023). https://doi.org/10.1016/j.csite.2023.102914

[21] Elboughdiri, N., Javid, K., Ahmed, I., et al., "Peristaltic pumping of hybrid nanofluid between concentric tubes with magnetic device effects: Applications to human endoscopy", *Journal of the Indian Chemical Society*, **99**(10), pp. 100710 (2022). https://doi.org/10.1016/j.jics.2022.100710

[22] Kumar, M.D., Raju, C., Shah, N.A., et al., "Support vector machine learning classification of heat transfer rate in tri-hybrid nanofluid over a 3D stretching surface with suction effects for water at 10° C and 50° C", *Alexandria Engineering Journal*, **118**, pp. 556-578 (2025). https://doi.org/10.1016/j.aej.2025.01.061

[23] Elboughdiri, N., Javid, K., Shehzad, M.Q., et al., "Influence of chemical reaction on electro-osmotic flow of nanofluid through convergent multi-sinusoidal passages", *Case Studies in Thermal Engineering*, **54**, pp. 103955 (2024). https://doi.org/10.1016/j.csite.2023.103955

[24] Raju, C., Ahammad, N.A., Sajjan, K., et al., "Nonlinear movements of axisymmetric ternary hybrid nanofluids in a thermally radiated expanding or contracting permeable Darcy Walls with different shapes and densities: Simple linear regression", *International Communications in Heat and Mass Transfer*, **135**, pp. 106110 (2022). https://doi.org/10.1016/j.icheatmasstransfer.2022.106110

[25] Dinesh Kumar, M., Siva Krishnam Raju, C., El-Zahar, E.R., et al., "Artificial neural network of thermal Buoyancy and Fourier flux impact on suction/injection-based Darcy medium surface filled with hybrid and ternary nanoparticles", *ZAMM-Journal of Applied Mathematics and Mechanics/Zeitschrift für Angewandte Mathematik und Mechanik*, **104**(4), pp. e202300618 (2024). https://doi.org/10.1002/zamm.202300618

[26] Elboughdiri, N., Salih, S.Q., Chauhan, B.S., et al., "Arc-curved microchannels engraved on segmented circular heat sink for heat transfer augmentation; ANN-based performance optimization", *Case Studies in Thermal Engineering*, **53**, pp. 103837 (2024). https://doi.org/10.1016/j.csite.2023.103837

[27] Talebi, F., Mahmoudi, A.H., and Shahi, M., "Numerical study of mixed convection flows in a square lid-driven cavity utilizing nanofluid", *International Communications in Heat and Mass Transfer*, **37**(1), pp. 79-90 (2010). https://doi.org/10.1016/j.icheatmasstransfer.2009.08.013

[28] Acharya, N., Maity, S., and Kundu, P.K., "Framing the hydrothermal features of magnetized TiO2–CoFe2O4 water-based steady hybrid nanofluid flow over a radiative revolving disk", *Multidiscipline Modeling in Materials and Structures*, (2019). https://doi.org/10.1108/MMMS-08-2019-0151

[29] Ahmad, S., Ali, K., and Ashraf, M., "MHD flow of Cu-Al 2 O 3/water hybrid nanofluid through a porous media", *Journal of Porous Media*, **24**(7) (2021). https://doi.org/10.1615/JPorMedia.2021036704

[30] Ahmad, S., Ali, K., Sajid, T., et al., "A novel vortex dynamics for micropolar fluid flow in a lid-driven cavity with magnetic field localization – A computational approach", *Ain Shams Engineering Journal*, pp. 102448 (2023). https://doi.org/10.1016/j.asej.2023.102448.

[31] Ahmad, S., Ali, K., Ayub, A., et al., "Localized magnetic fields and their effects on heat transfer enhancement and vortices generation in tri-hybrid nanofluids: A novel investigation", *Case Studies in Thermal Engineering*, pp. 103408 (2023). https://doi.org/10.1016/j.csite.2023.103408

[32] Ahmad, S., Takana, H., Ali, K., et al., "Role of localized magnetic field in vortex generation in tri-hybrid nanofluid flow: A numerical approach", *Nanotechnology Reviews*, **12**(1), pp. 20220561 (2023). https://doi.org/10.1515/ntrev-2022-0561

[33] Ahmad, S., Takana, H., Castellanos, H.G., et al., "Uncovering the mystery of the vortex dynamics in a micropolar fluid with multiple magnetic field strips: A novel case study", *Case Studies in Thermal Engineering*, pp. 103716 (2023). https://doi.org/10.1016/j.csite.2023.103716

[34] Ahmad, S., Santos, E.D.d., Ali, K., et al., "The role of machine learning in analyzing magnetic field localization and vortex generation in tetra-hybrid nanofluid: A numerical study", *Modern Physics Letters B*, pp. 2550115 (2025). https://doi.org/10.1142/S0217984925501155

Figures presented in the manuscript are listed below in numerical order, corresponding to the sequence in which they are cited within the text

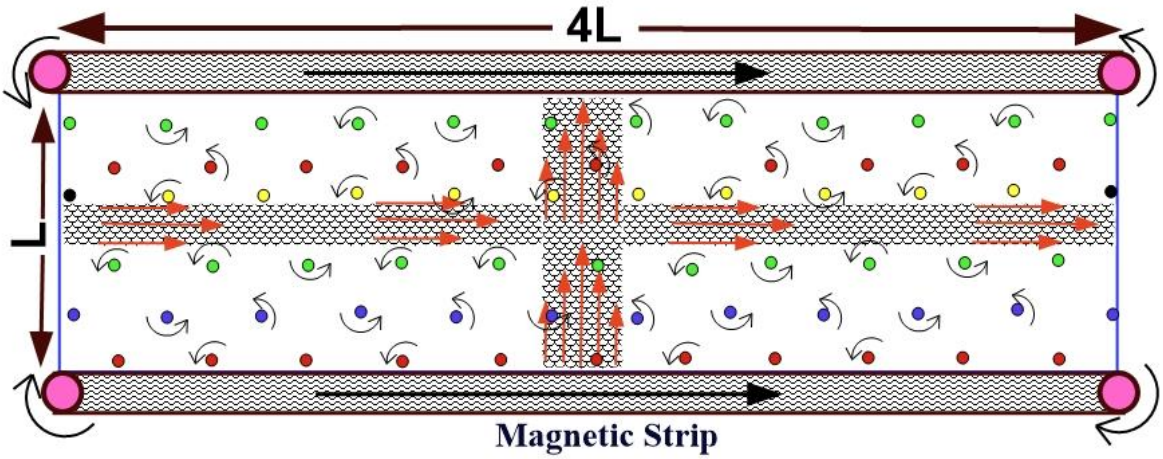

Fig. 1. Illustration of Magnetic Field Sections Using Straight Arrows.

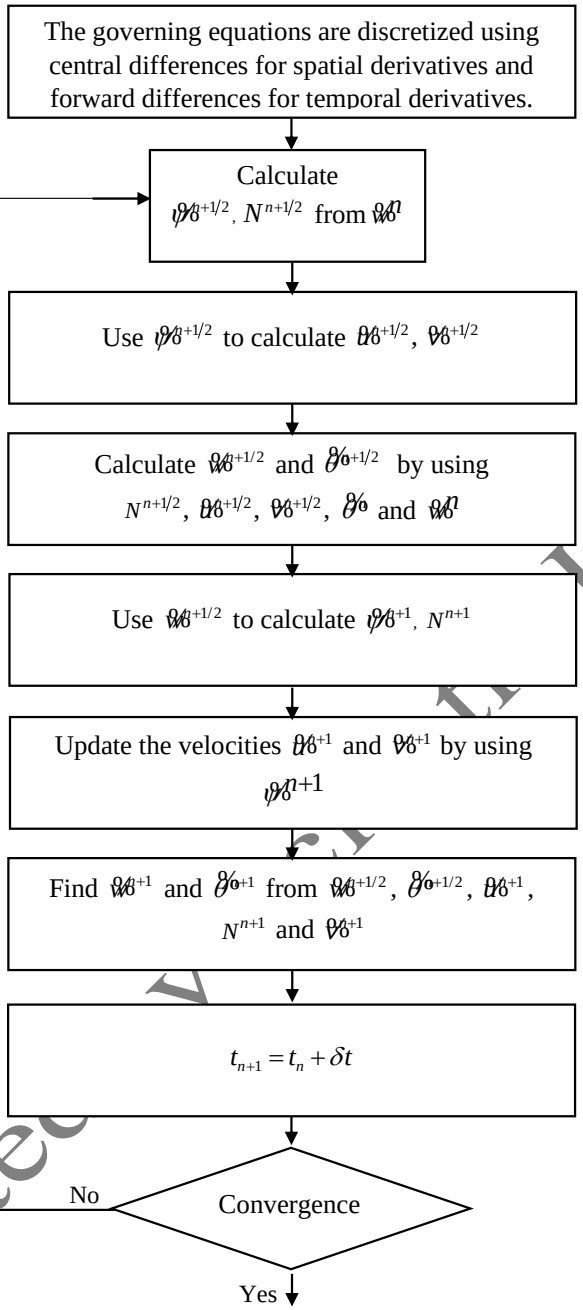

Fig. 2. A Flow Chart Regarding Pseudo-Transient Scheme.

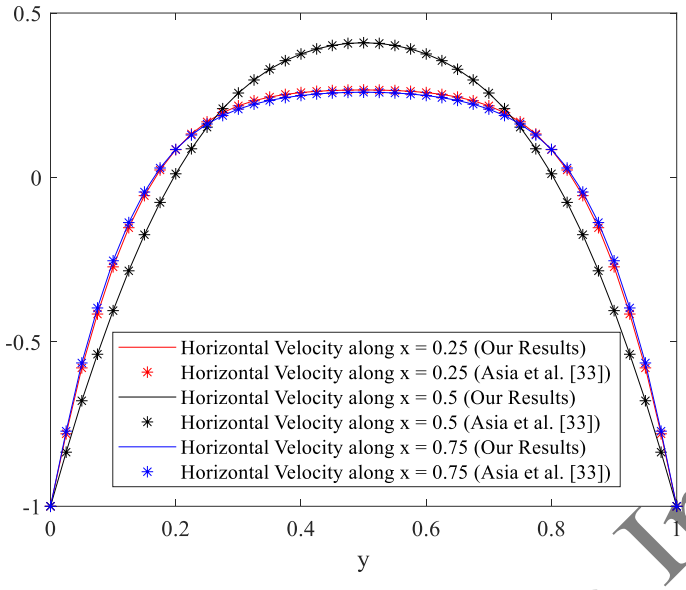

Fig. 3. Validation of Numerical Results against the Analytical Method of Asia et al. [33].

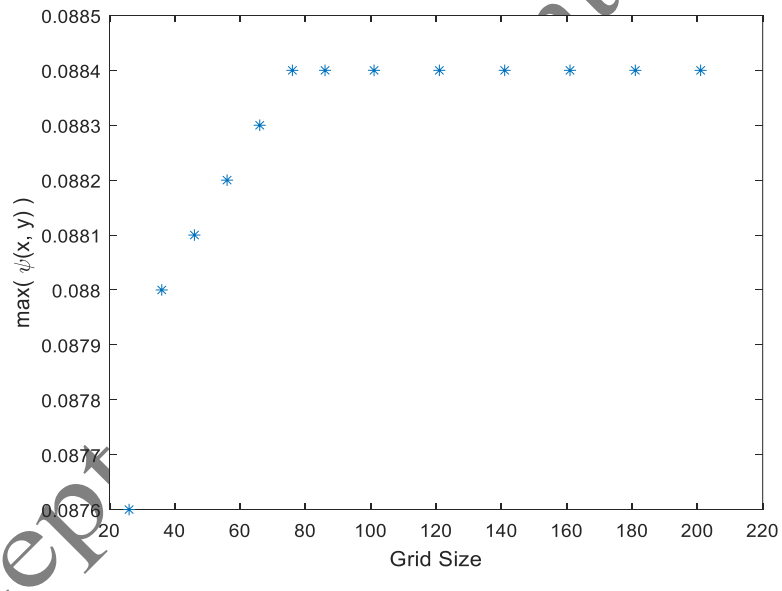

Fig. 4. Grid Independence Study.

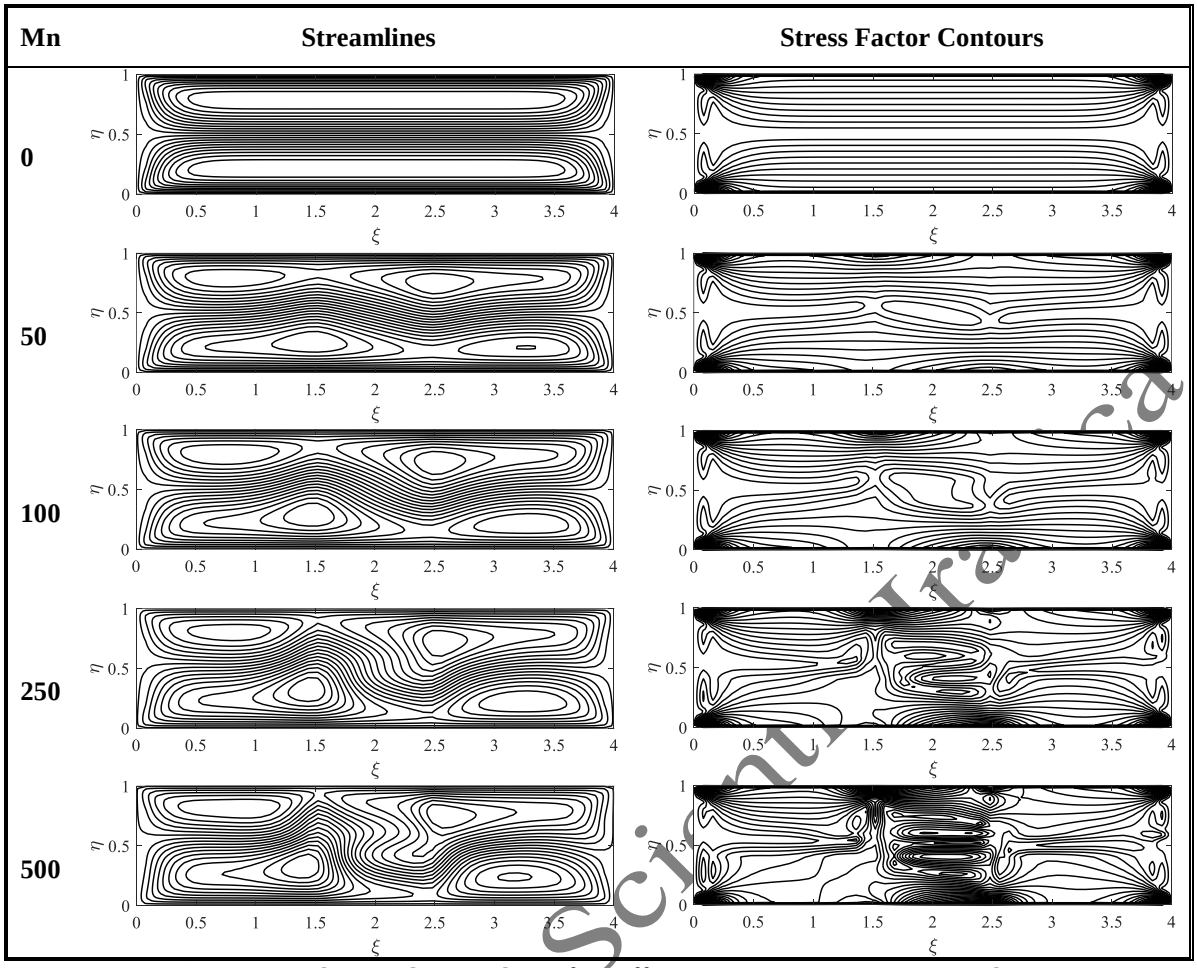

Fig. 5. Streamlines and its Gradients for Different Mn at Pr = 6.8, Re = 3, and C = 1.

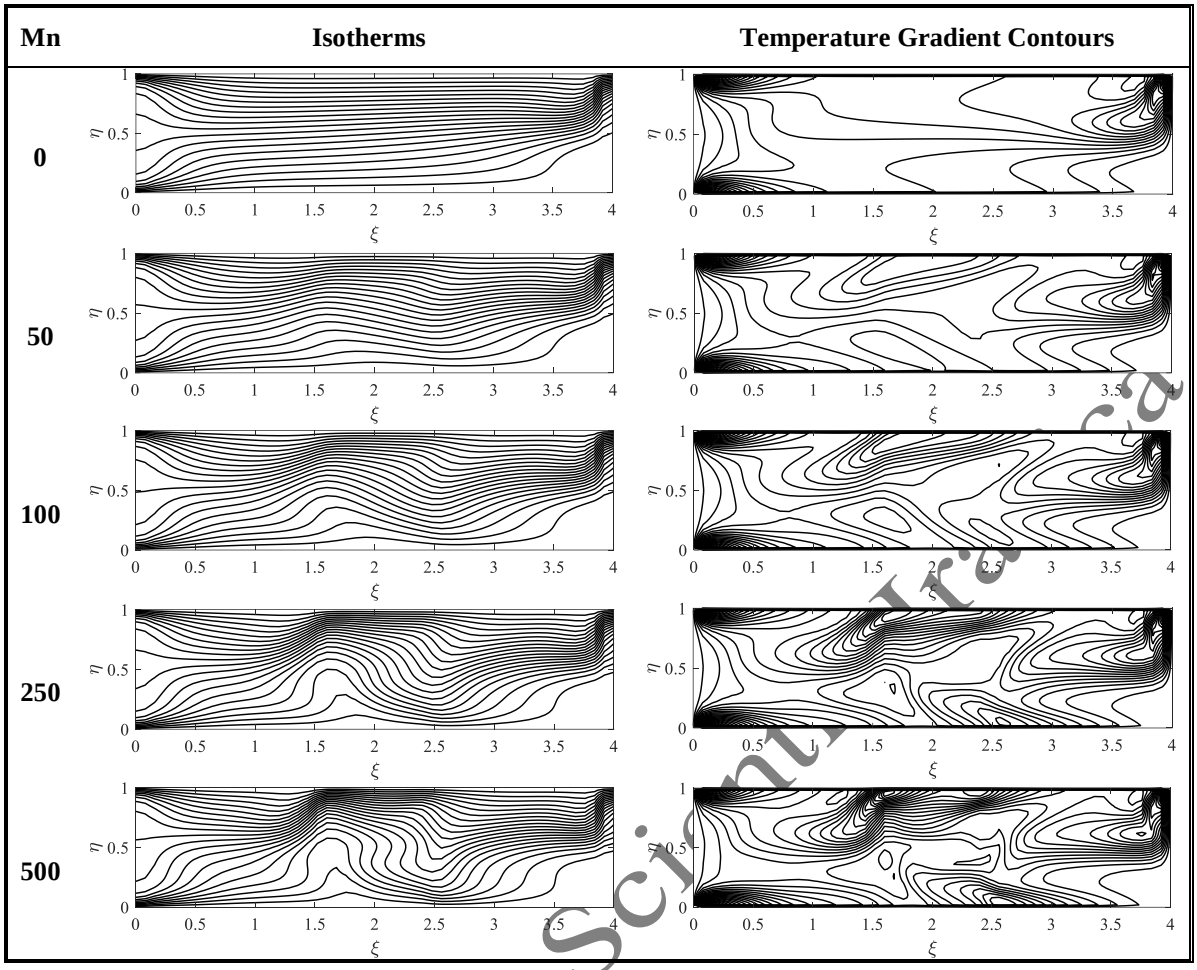

Fig. 6. Isotherms and its Gradients for Different Mn at Pr = 6.8, Re = 3, and C = 1.

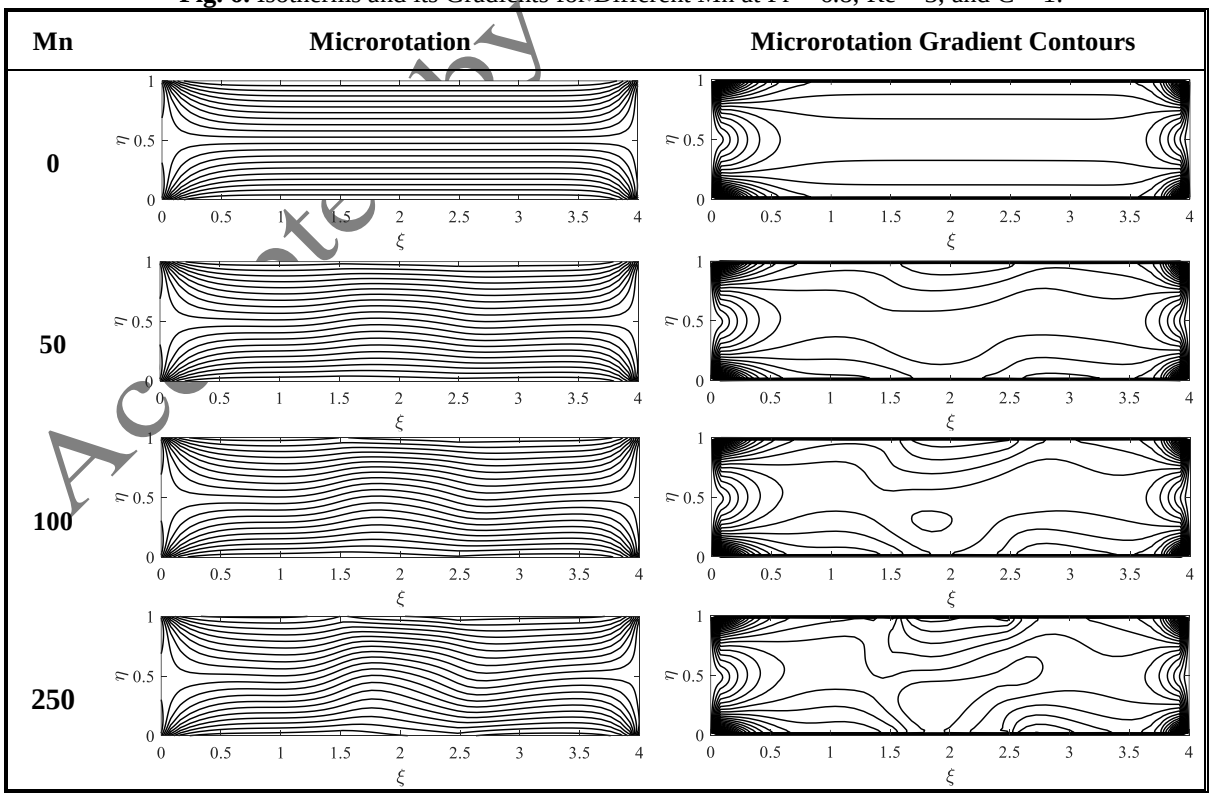

Fig. 7. Microrotation and its Gradients for Different Mn at Pr = 6.8, Re = 3, and C = 1.

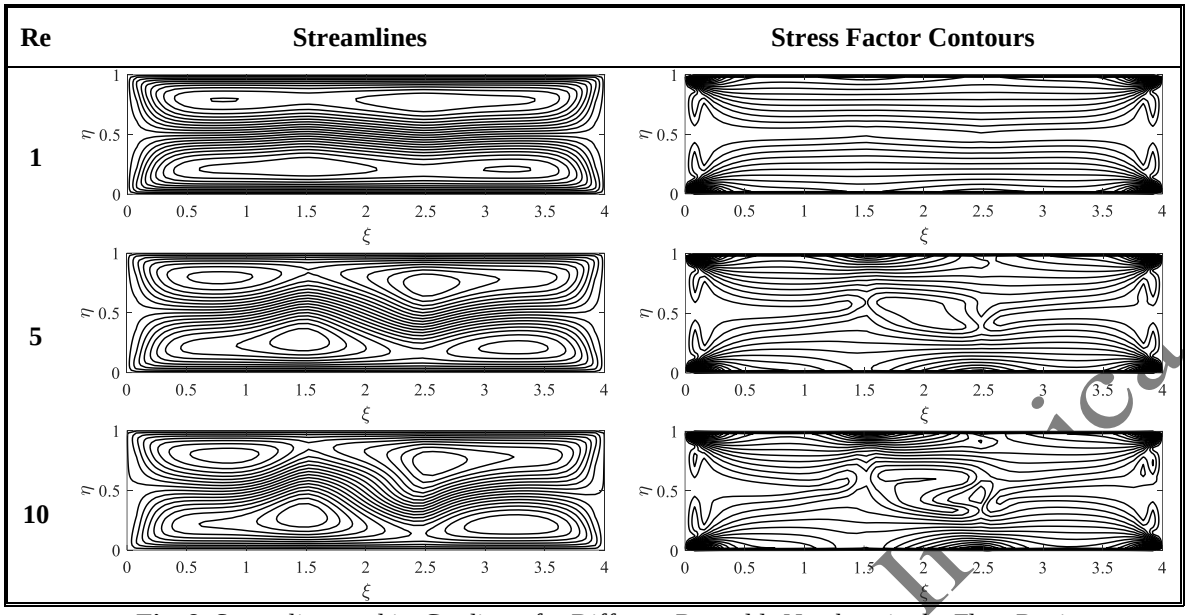

Fig. 8. Streamlines and its Gradients for Different Reynolds Numbers in the Flow Regime.

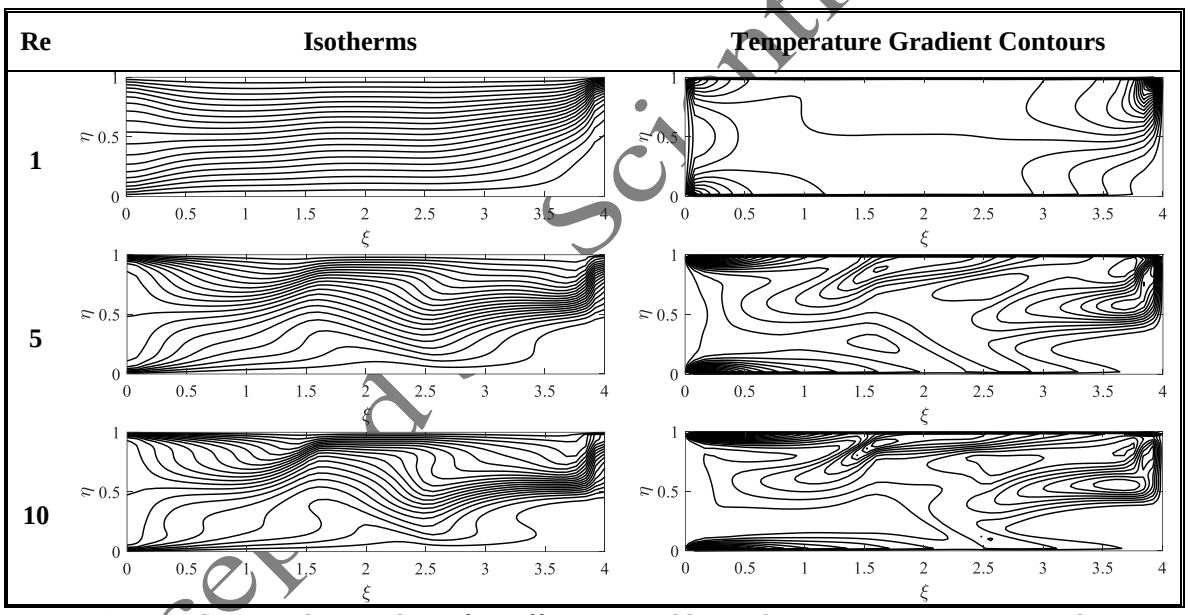

Fig. 9. Isotherms and its Gradients for Different Reynolds Numbers at Pr = 6.8, Mn = 50, and C = 1.

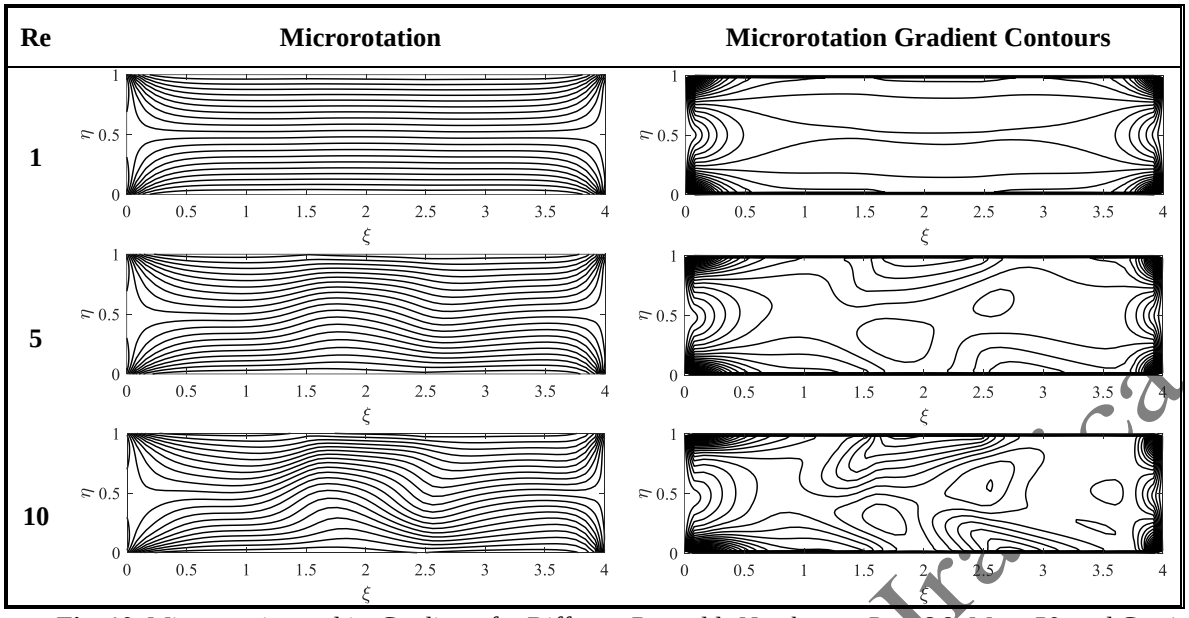

Fig. 10. Microrotation and its Gradients for Different Reynolds Numbers at Pr = 6.8, Mn = 50, and C = 1.

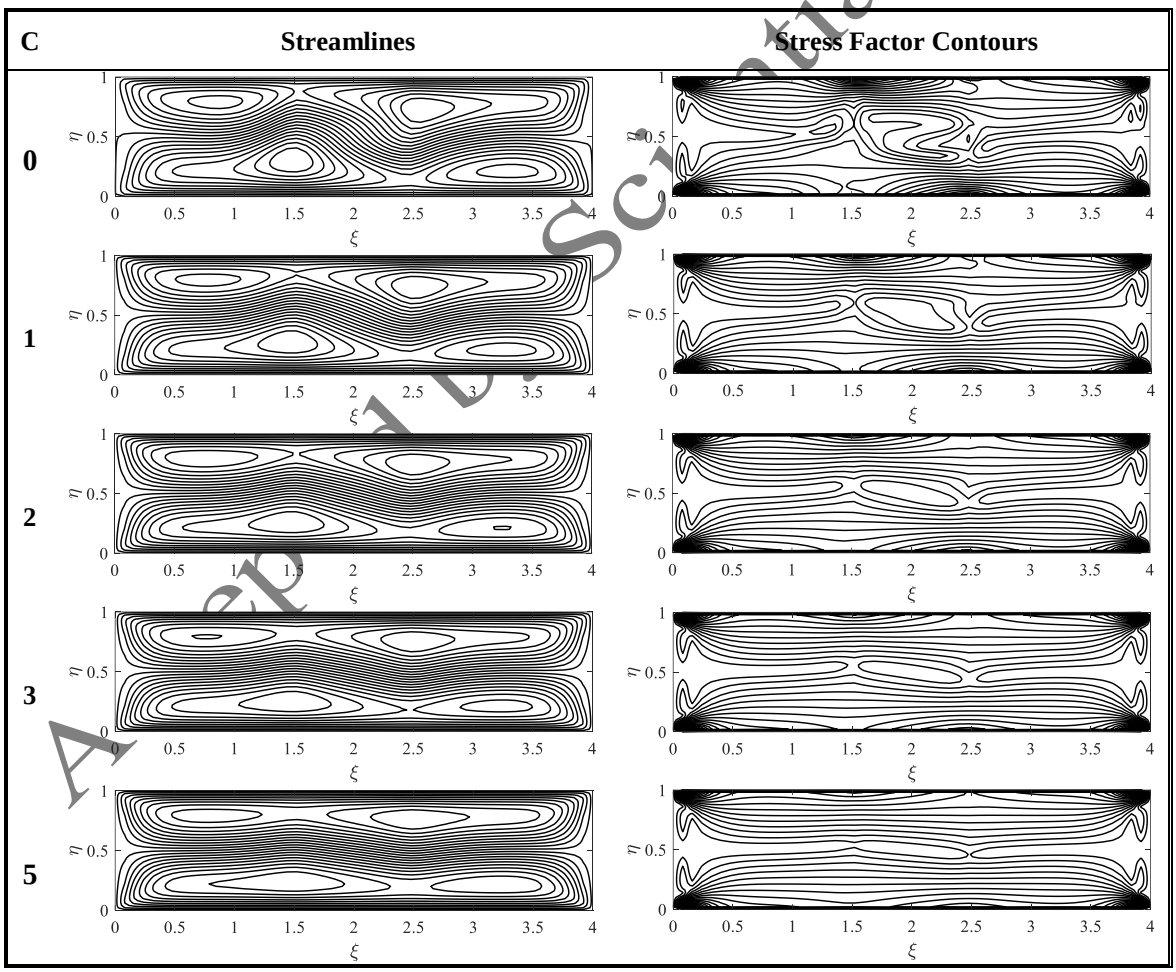

Fig. 11. Streamlines and its Gradients for Different Microrotation Parameter (C) at Re = 5, Mn = 50, and Pr = 6.8.

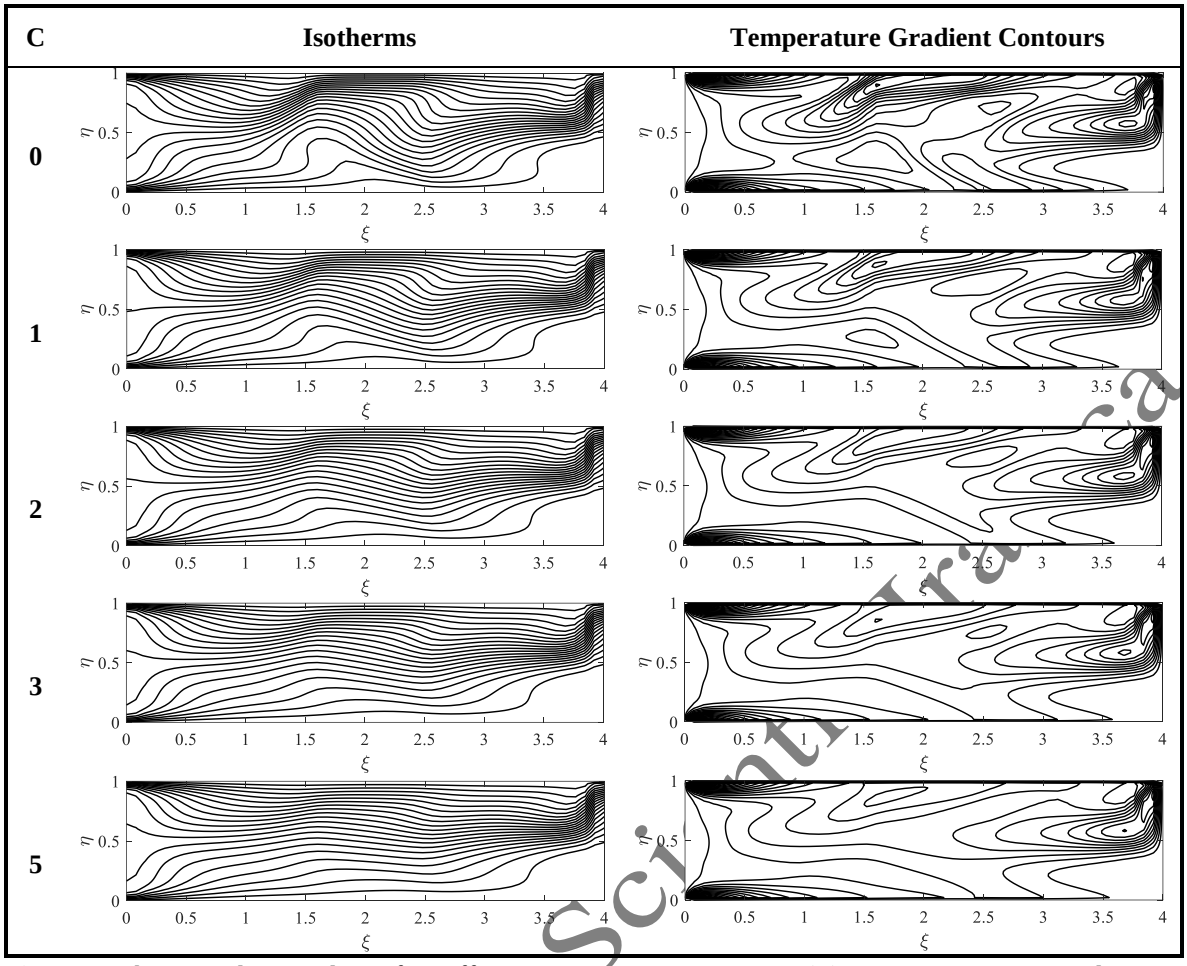

Fig. 12. Isotherms and its Gradients for Different Microrotation Parameter (C) at Re = 5, Mn = 50, and Pr = 6.8.

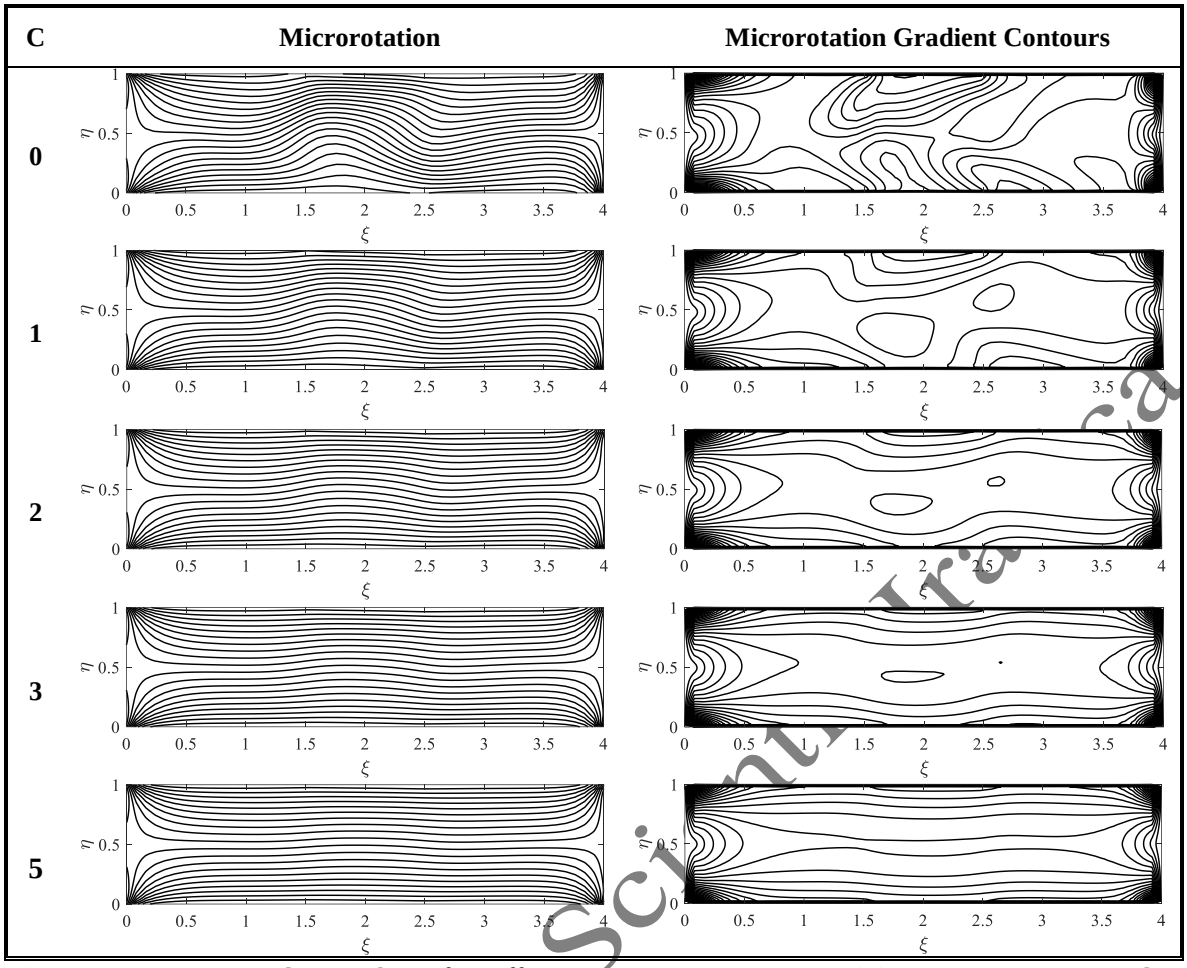

Fig. 13. Microrotation and its Gradients for Different Microrotation Parameter (C) at Re = 5, Mn = 50, and Pr = 6.8.

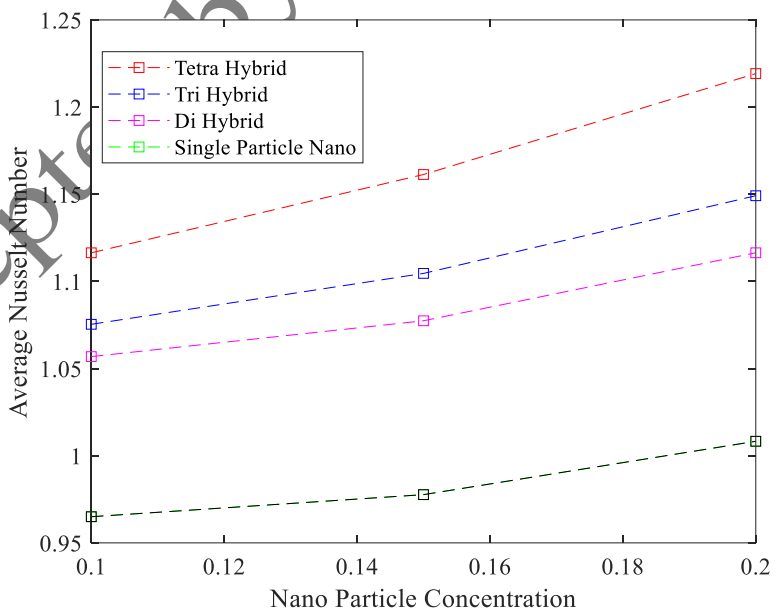

Fig. 14. Assessing Hybrid Nanofluid in Comparison to the Tetra-hybrid Nanoparticles.

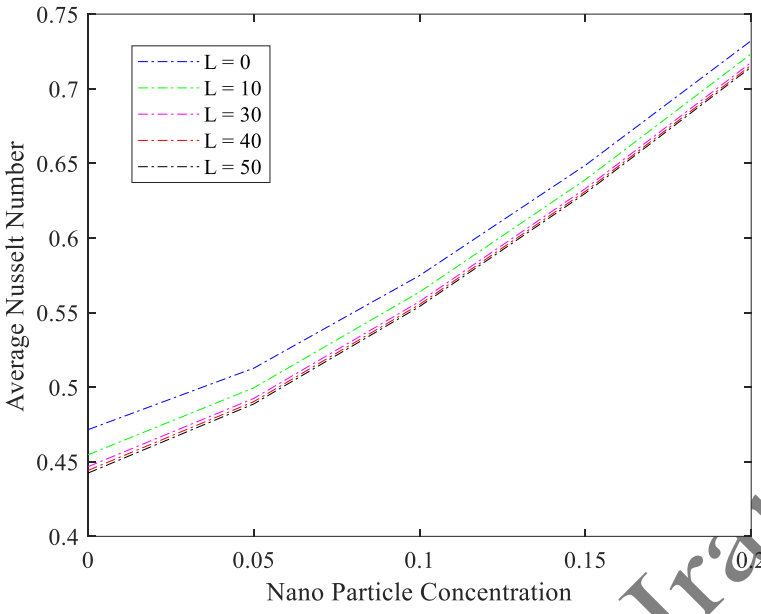

Fig. 15. Effect of Magnetic Strip on the Average Nu.

Tables presented in the manuscript are listed below in numerical order, corresponding to the sequence in which they are cited within the text

Table 1. Thermophysical Property Comparison between Tetra-Hybrid and Traditional Nanofluids [34].

Properties	**Tetra-hybrid microfluid**
Density	$\rho_{tet\_hnf} = \left\{(1-\phi_4)\left((1-\phi_3)\left[(1-\phi_1)\left\{(1-\phi_2)\rho_f + \phi_1\rho_{s1}\right\} + \phi_2\rho_{s2}\right] + \phi_3\rho_{s3}\right) + \phi_4\rho_{s4}\right\}$
Heat capacity	$(\rho c_p)_{tet\_hnf} = \left\{\begin{array}{l}(1-\phi_4)\left(\begin{array}{l}(1-\phi_3)\left[(1-\phi_1)\left\{(1-\phi_2)C_{pf}\rho_f + \phi_1 C_{ps1}\rho_{s1}\right\} + \phi_2 C_{ps2}\rho_{s2}\right] \\ +\phi_3 C_{ps3}\rho_{s3}\end{array}\right) \\ +\phi_4 C_{ps4}\rho_{s4}\end{array}\right\}$
Viscosity	$\mu_{tet\_hnf} = \frac{\mu_f}{(1-\phi_1)^{2.5}(1-\phi_2)^{2.5}(1-\phi_3)^{2.5}(1-\phi_4)^{2.5}}$
Thermal conductivity	$\frac{k_{tet\_hnf}}{k_{thnf}} = \frac{k_{s4} + (n-1)(k_{thnf} - (n-1)\phi_{s4})(k_{thnf} - k_{s4})}{k_{s4} + (n-1)k_{thnf} + \phi_{s4}(k_{thnf} - k_{s4})}$ $\frac{k_{thnf}}{k_{hnf}} = \frac{k_{s3} + (n-1)(k_{hnf} - (n-1)\phi_{s3})(k_{hnf} - k_{s3})}{k_{s3} + (n-1)k_{hnf} + \phi_{s3}(k_{hnf} - k_{s3})}$ where $\frac{k_{hnf}}{k_{nf}} = \frac{k_{s2} - (n-1)\phi_2(k_{nf} - k_{s3}) + (n-1)k_{nf}}{k_{s2} + \phi_{s2}(k_{nf} - k_{s3}) + (n-1)k_{nf}}$ and $\frac{k_{nf}}{k_f} = \frac{k_{s1} - (n-1)\phi_1(k_f - k_{s1}) + (n-1)k_f}{k_{s1} + \phi_1(k_f - k_{s1}) + (n-1)k_f}$
Electric conductivity	$\frac{\sigma_{tet\_hnf}}{\sigma_{thnf}} = \frac{\sigma_{s4} - 2\phi_4(\sigma_{thnf} - \sigma_{s4}) + 2\sigma_{thnf}}{\sigma_{s4} + \phi_4(\sigma_{thnf} - \sigma_{s4}) + 2\sigma_{thnf}}$ $\frac{\sigma_{thnf}}{\sigma_{hnf}} = \frac{\sigma_{s3} - 2\phi_3(\sigma_{hnf} - \sigma_{s3}) + 2\sigma_{hnf}}{\sigma_{s3} + \phi_3(\sigma_{hnf} - \sigma_{s3}) + 2\sigma_{hnf}}$ where $\frac{\sigma_{hnf}}{\sigma_{nf}} = \frac{\sigma_{s2} - 2\phi_2(\sigma_{nf} - \sigma_{s2}) + 2\sigma_{nf}}{\sigma_{s2} + \phi_2(\sigma_{nf} - \sigma_{s2}) + 2\sigma_{nf}}$ and $\frac{\sigma_{nf}}{\sigma_f} = \frac{\sigma_{s1} - 2\phi_1(\sigma_f - \sigma_{s1}) + 2\sigma_f}{\sigma_{s1} + \phi_1(\sigma_f - \sigma_{s1}) + 2\sigma_f}$

Table 2. Analysis of Thermophysical Behavior of Ag-SWCNT-TiO_2-Cu Nanofluids in a Water Base.

	$C_p(Jkg^{-1}K^{-1})$	$\beta(K^{-1})$	$\hat{\rho}(kgm^{-3})$	$\sigma(S \times m^{-1})$	$k(Wm^{-1}K^{-1})$
Silver (Ag)	235	1.89×10^{-5}	10.5	3.6×10^{7}	429
SWCNT	425	0.85×10^{-5}	2600	1×10^{6}	6600
Titanium oxide (TiO_2)	670	1.3	5200	25,000	6
Copper (Cu)	385	1.67×10^{-5}	8933	5.96×10^{7}	401
Water	4179	21×10^{-5}	997.1	5.5×10^{-6}	0.613

Table 3. Examining the Impact of Mn on Nu, and CfRe, at C=1, Re = 1, and Mn = 3.

Mn	$\lvert Nu \rvert$	$\lvert$CfRe$\rvert$
0	0.366	0.009
100	0.386	1.191
200	0.426	2.179
300	0.454	3.743
500	0.602	9.116

Table 4. Examining the Impact of Re on Nu, and CfRe, at C=1, Re = 1, and Mn = 3.

Re	$\lvert Nu \rvert$	$\lvert$CfRe$\rvert$
01	0.280	0.056
02	0.519	0.272
04	0.876	0.814
06	1.061	1.583
10	1.870	2.652

Table 5. Examining the Impact of Microrotation on Nu, and CfRe, at C=1, Re = 1, and Mn = 3.

C	$\lvert Nu \rvert$	$\lvert$CfRe$\rvert$
0.0	0.817	2.103
1.0	0.723	1.087
2.0	0.677	0.701
3.0	0.531	0.589
5.0	0.416	0.438

Table 6. Examining the Impact of Silver Particles on Nu, and CfRe, at C=1, Re = 1, and Mn = 3.

ϕ_1 (Silver)	$\lvert Nu \rvert$	$\lvert$CfRe$\rvert$
0.00	0.380	0.097
0.05	0.529	0.071
0.10	0.856	0.057
0.15	1.061	0.046
0.20	1.570	0.033

Table 7. Examining the Impact of SWCNT on Nu, and CfRe, at C=1, Re = 1, and Mn = 3.

ϕ_2 (SWCNT)	$\lvert Nu \rvert$	$\lvert$CfRe$\rvert$
0.00	0.324	0.071
0.05	0.353	0.081
0.10	0.414	0.095
0.15	0.453	0.115
0.20	0.500	0.172

Table 8. Examining the Impact of Titanium Dioxide Particles on Nu, and CfRe, at C=1, Re = 1, and Mn = 5.

ϕ_3 (Titanium Dioxide)	$\lvert Nu \rvert$	$\lvert$CfRe$\rvert$
0.00	0.323	0.096
0.05	0.357	0.067
0.10	0.405	0.054
0.15	0.441	0.033
0.20	0.464	0.024

Table 9. Examining the Impact of Copper Particles on Nu, and CfRe, at C=1, Re = 1, and Mn = 3.

ϕ_4 (Copper)	$\lvert Nu \rvert$	$\lvert$CfRe$\rvert$
0.00	0.365	0.090
0.05	0.388	0.082
0.10	0.396	0.066
0.15	0.414	0.052
0.20	0.478	0.043

Dr. Shabbir Ahmad earned his M.Sc. in Mathematics from Government College University, Faisalabad, Pakistan, in 2006, and his Ph.D. in Geophysics from the China University of Geosciences, Wuhan, China, in 2021. He began his academic career as a Visiting Professor at the Federal University of Rio Grande, Brazil. He has published more than 55 research papers in reputable international journals. His research interests include computational fluid dynamics and heat transfer, particularly nanofluids, hybrid and tri-hybrid nanofluids under localized magnetic fields. His work also explores vortex dynamics, magnetohydrodynamics, porous media, and thermodynamic system optimization, including geothermal and solar-powered technologies.

Dr. Elizaldo Domingues dos Santos graduated in Mechanical Engineering from the Federal University of Rio Grande (FURG) in 2004 and earned his Master's (2007) and Ph.D. (2011) in Mechanical Engineering from the Federal University of Rio Grande do Sul (UFRGS). He is an Associate Professor at FURG and a permanent faculty member of the Graduate Programs in Computational Modeling and Ocean Engineering. He has extensive experience in fluid mechanics, heat transfer, thermodynamics, renewable energy, and computational fluid dynamics. He has served in leadership roles at FURG, including Graduate Studies Director and coordinator of the Ocean Engineering Graduate Program. His main research areas include turbulent flow analysis, convective heat transfer, renewable energy devices, and constructal design.

Dr. Kashif Ali is an Associate Professor and Head of the Department of Basic Sciences and Humanities at Muhammad Nawaz Sharif University of Engineering and Technology, Multan, Pakistan. He received his Ph.D. in Mathematics from Bahauddin Zakariya University, Multan, in 2016. His research focuses on computational fluid dynamics, heat and mass transfer in complex fluids, micropolar and non-Newtonian fluids, nanofluids, porous media, and magnetohydrodynamics. He has published over 85 peer-reviewed journal articles and employs advanced numerical methods to study multiphysics problems relevant to engineering and environmental systems.

Dr. Moin-ud-Din Junjua is a Postdoctoral Fellow at Zhejiang Normal University, China. He obtained his Ph.D. in Computational Mathematics from Bahauddin Zakariya University, Multan, Pakistan, in 2019. With over a decade of academic experience, he has previously served as an Assistant Professor and Ph.D. supervisor at Ghazi University, Pakistan. His research interests include iterative methods for nonlinear equations, computational mathematics, and fractal dynamics. He has published more than 45 research papers and presented at several international conferences. He has also supervised over 30 postgraduate students.

Dr. Farhan Lafta Rashid earned his B.Sc. in Nuclear Engineering from the University of Baghdad, Iraq, in 1994, his M.Sc. in Thermo-Fluid Mechanics in 2002, and his Ph.D. in 2016 from the University of Technology, Iraq. He began his career at the Iraqi Atomic Energy Commission and is currently a Professor of Fluid Mechanics and Thermodynamics at the University of Kerbala. He has authored more than 255 research papers and holds eleven patents. His research focuses on computational fluid dynamics, fluid flow analysis, modeling, and simulation.

Dr. Ahmed S. Hendy is a Senior Researcher in Computational Mathematics and Computer Science at Ural Federal University, Russia, and a faculty member at Benha University, Egypt. His research spans computational fluid dynamics, nanofluid dynamics, fractional differential equations, and biomedical applications. He has contributed significantly to the study of vortex generation in nanofluids, heat and mass transfer, and the integration of machine learning into multiphysics modeling. He has also applied computational methods to health-related studies, including antibiotic resistance and pediatric malnutrition.

Prof. Dr. Noureddine Elboughdiri is a Professor and Head of the Chemical Engineering Department at Hail University, Saudi Arabia. He received his B.Sc., Master's, and Ph.D. in Chemical Engineering from the University of Gabes, Tunisia. He has held positions in industry and academia, including work with the Central Laboratory for Analysis and Testing and the SGS Group. His research focuses on wastewater treatment, artificial neural networks, and Aspen Plus simulation. He has extensive experience in academic accreditation and quality assurance systems.

Dr. Saad A. Alshahrani is an Associate Professor in Mechanical Engineering and Director of the Center for Engineering and Technology Innovations at King Khalid University, Saudi Arabia. He earned his Ph.D. and M.Sc. in Mechanical Engineering from Michigan State University, USA. His research interests include renewable energy systems, supercritical CO_2 power cycles, solar energy conversion, heat pumps, sustainable biofuels, and water desalination. He has authored numerous journal articles, contributed to conferences, and holds a patent on solar-based power generation. He is an active member of ASME, ASHRAE, ASTFE, and the Saudi Council of Engineers.